Cell Reports Medicine, Volume *3*

Supplemental information

A molecularly engineered, broad-spectrum anti-coronavirus lectin inhibits SARS-CoV-2 and MERS-CoV infection *in vivo*

Jasper Fuk-Woo Chan, Yoo Jin Oh, Shuofeng Yuan, Hin Chu, Man-Lung Yeung, Daniel Canena, Chris Chung-Sing Chan, Vincent Kwok-Man Poon, Chris Chun-Yiu Chan, Anna Jinxia Zhang, Jian-Piao Cai, Zi-Wei Ye, Lei Wen, Terrence Tsz-Tai Yuen, Kenn Ka-Heng Chik, Huiping Shuai, Yixin Wang, Yuxin Hou, Cuiting Luo, Wan-Mui Chan, Zhenzhi Qin, Ko-Yung Sit, Wing-Kuk Au, Maureen Legendre, Rong Zhu, Lisa Hain, Hannah Seferovic, Robert Tampé, Kelvin Kai-Wang To, Kwok-Hung Chan, Dafydd Gareth Thomas, Miriam Klausberger, Cheng Xu, James J. Moon, Johannes Stadlmann, Josef M. Penninger, Chris Oostenbrink, Peter Hinterdorfer, Kwok-Yung Yuen, and David M. Markovitz

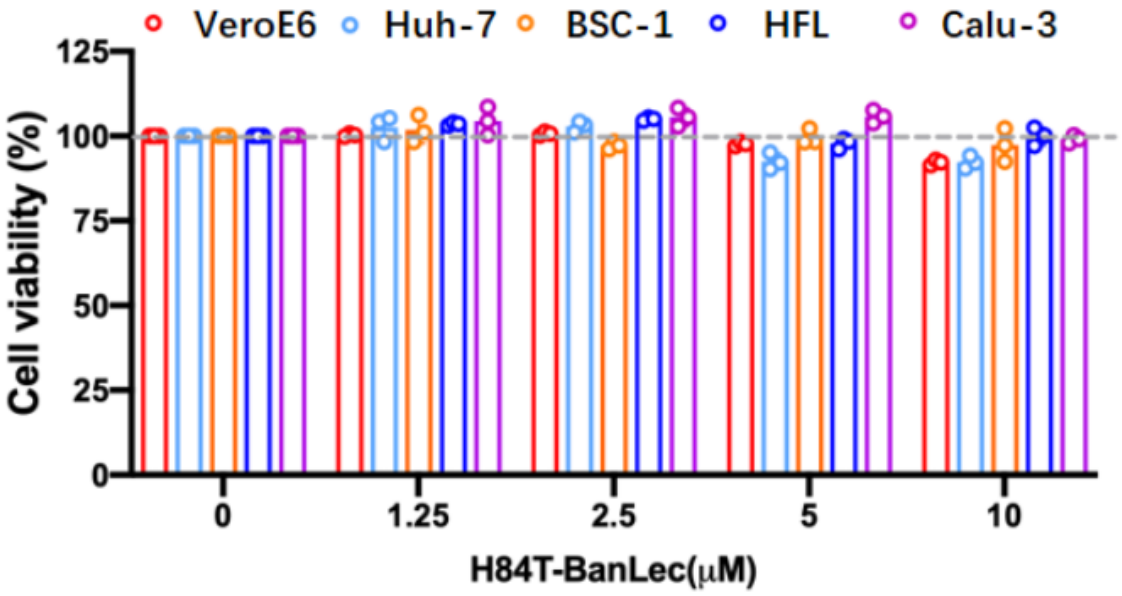

Figure S1. The cytotoxicity of H84T-BanLec in different cell lines. The cytotoxicity of H84T-BanLec in VeroE6, Huh7, BSC-1, HFL, and Calu-3 cells was evaluated using the CellTiterGlo® luminescent cell viability assay according to manufacturer's instructions. H84T-BanLec did not display any obvious cytotoxicity in any of these cell lines even at the concentration of 10μM (ie: 10,000nM). Related to Figure 1.

(A)

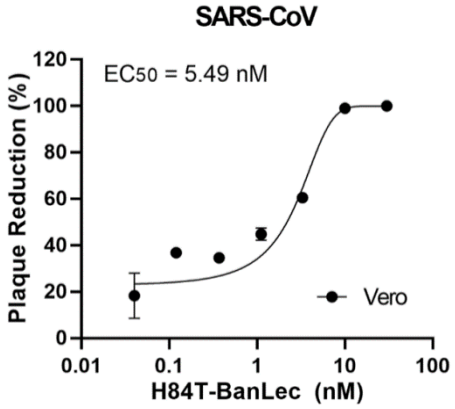

(B)

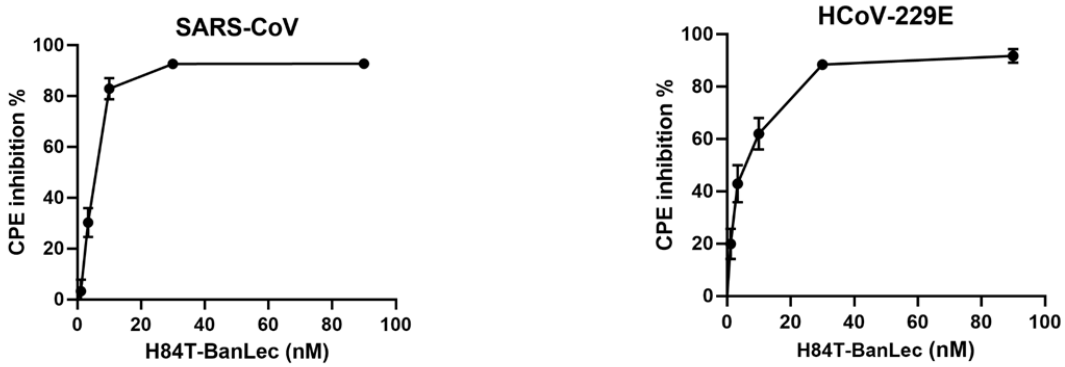

Figure S2. Antiviral activity of H84T-BanLec against other human-pathogenic coronaviruses. The antiviral activity of H84T-BanLec against SARS-CoV by **A,** plaque reduction assay and **B, (left)** CPE inhibition assay; and **B, (right)** against HCoV-229E by CPE inhibition assay. Related to Figure 1.

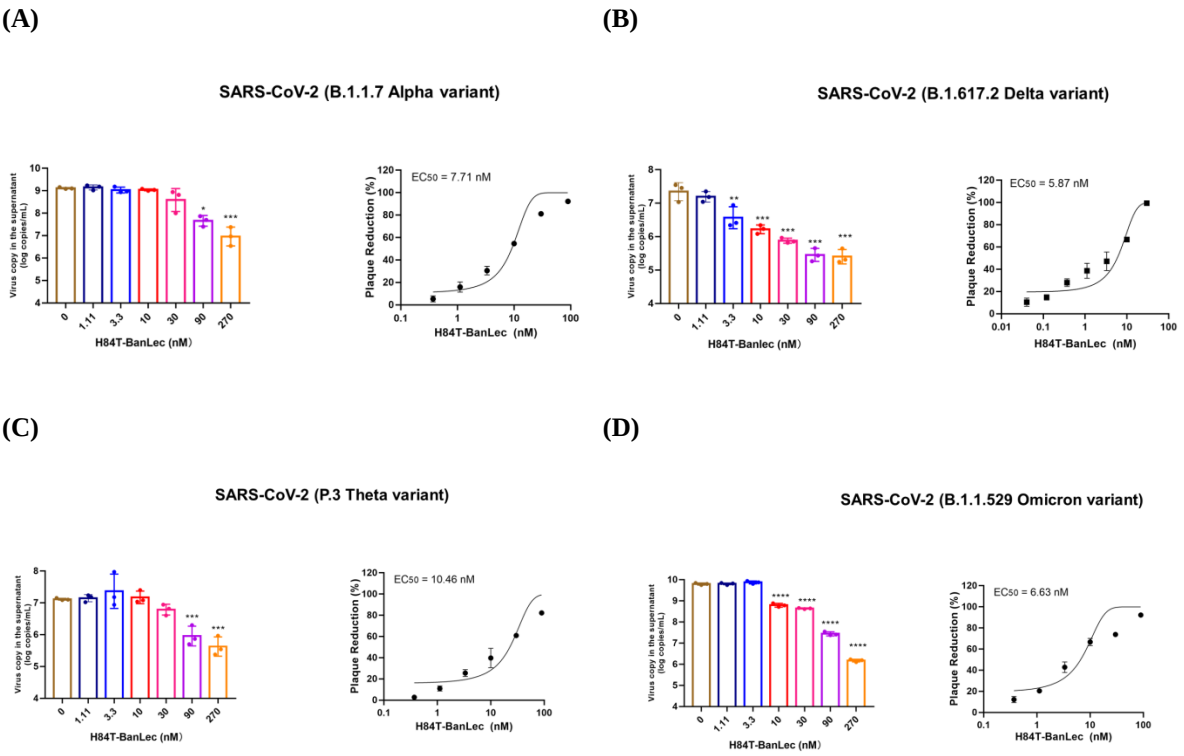

Figure S3. Antiviral activity of H84T-BanLec against emerging SARS-CoV-2 variants. The antiviral activity of H84T-BanLec against SARS-CoV-2: **A,** B.1.1.7 (Alpha, with N501Y), **B,** B.1.617.2 (Delta), **C,** P.3 (Theta, with N501Y, E484K, and 141 to 143 deletion), and **D,** B.1.1.529 (Omicron) variants were evaluated by **(left)** viral load reduction and **(right)** plaque reduction assays in VeroE6-TMPRSS2 cells. Data are mean ± s.d., n = 3 biological replicates. One-way ANOVA. ***P<0.001, **P<0.01, *P<0.05. Related to Figure 1.

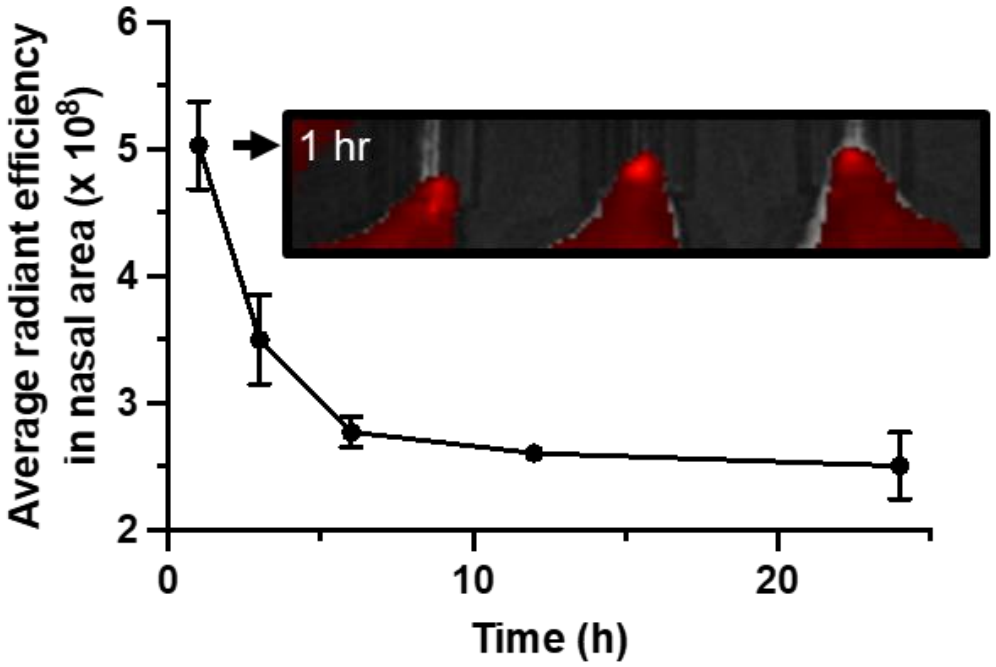

Figure S4. Intranasal delivery of H84T-BanLec. BALB/c mice were administered AF647-tagged H84T-BanLec intranasally. Mice were visualized by *in vivo* fluorescence imaging over 24 hours, and the fluorescence signal in the nasal area was quantified. Related to Figures 2 and 3.

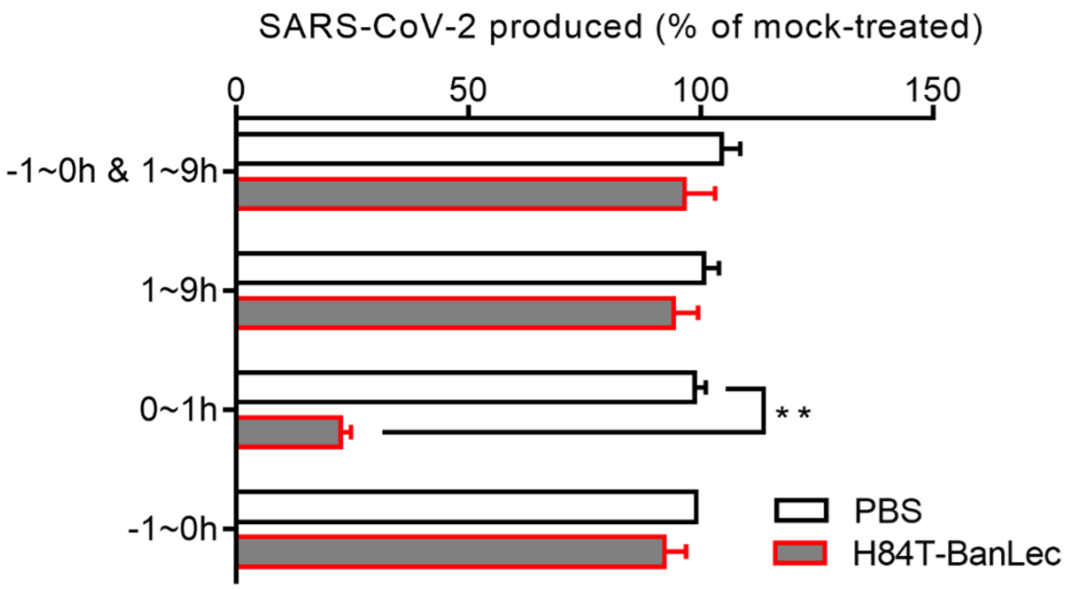

Figure S5. H84T-BanLec targets SARS-CoV-2 entry. Time-of-drug-addition assay indicated that H84T-BanLec interfered with SARS-CoV-2 entry. Student's t-test. ***P*<0.01. Related to Figures 1 to 3.

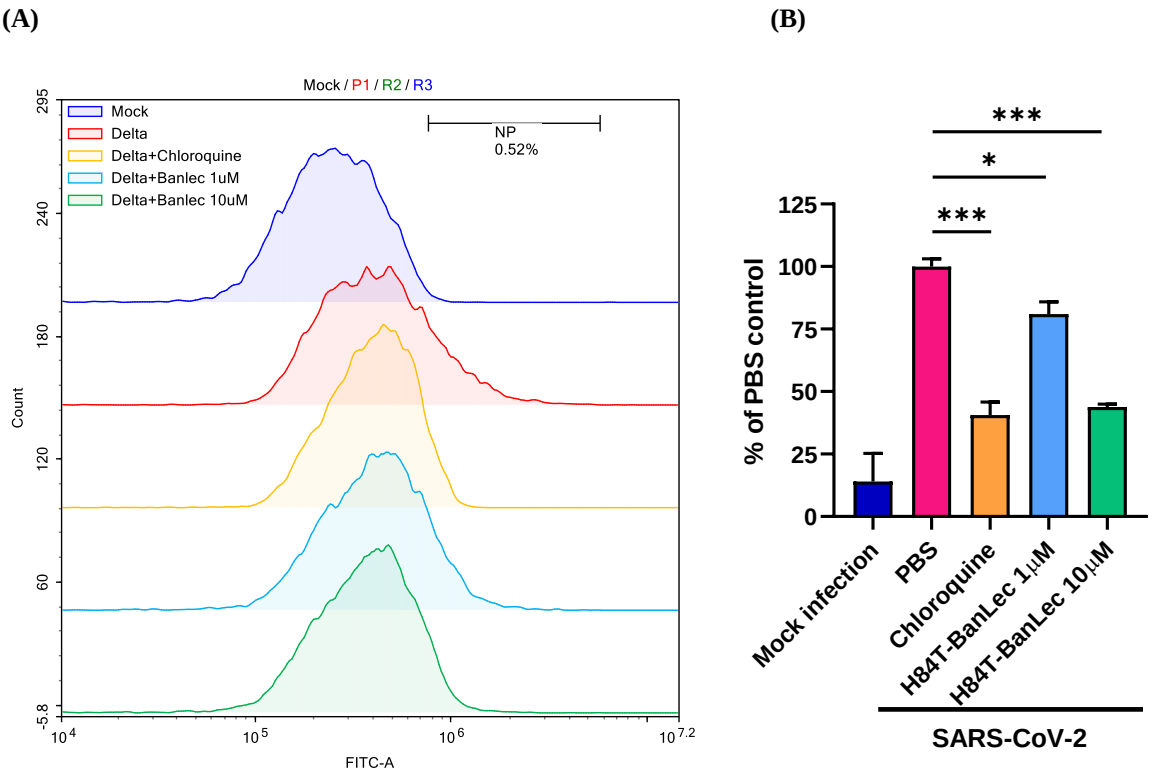

Figure S6. Detection of SARS-CoV-2 entry by flow cytometry. A, Representative histograms of mock- or SARS-CoV-2-infected cells (MOI = 1.0) permeabilized and then quantified by fluorescein isothiocyanate (FITC) staining after anti-SARS-CoV-2 nucleocapsid protein antibody and then anti-Alexa Flour 488 conjugated secondary antibody were added. The median fluorescence intensity (MFI) of each group is shown. **B,** SARS-CoV-2 nucleocapsid protein-positive cells were quantified after H84T-BanLec or PBS treatment. The results were shown as mean ± SD of the PBS control and in triplicate. One-way ANOVA. ***P<0.001, *P<0.05. Related to Figures 1 to 3.

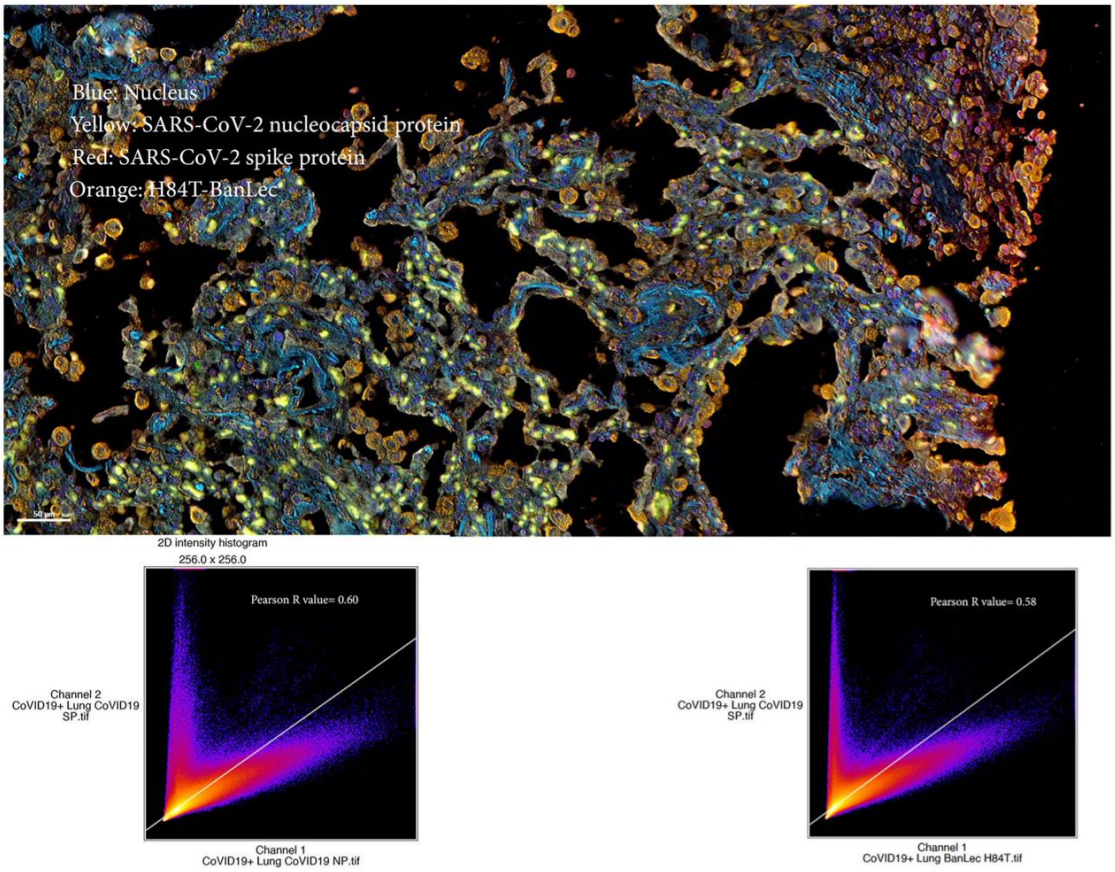

Figure S7. Co-localization of H84T-BanLec with SARS-CoV-2 spike protein in the autopsied lung section of a deceased COVID-19 patient. Top, Multiplex immunohistochemical analysis of SARS-CoV-2-infected autopsy lung section (SARS-CoV-2 nucleocapsid protein, yellow; SARS-CoV-2 spike protein, red; and H84T-BanLec, orange). Total original magnification 200×. Sections were counterstained with DAPI to visualize nuclei (blue) and scanned using the Polaris Vectra multiplex spectral scanner. **Bottom,** The digital metadata were uploaded to FIJI for co-localization. The mean pixel intensity for each fluorochrome (0-256) at a particular centroid was plotted and the number of co-localizations calculated. The Pearson correlation calculation ranged from -1 to +1 and indicated inverse correlation (-1) through no correlation (0) to positive correlation (+1). The values calculated (0.6 and 0.58) for spike protein vs nucleocapsid protein and spike protein versus H84T-BanLec respectively represented high degrees of co-localization. Related to Figures 1 to 3.

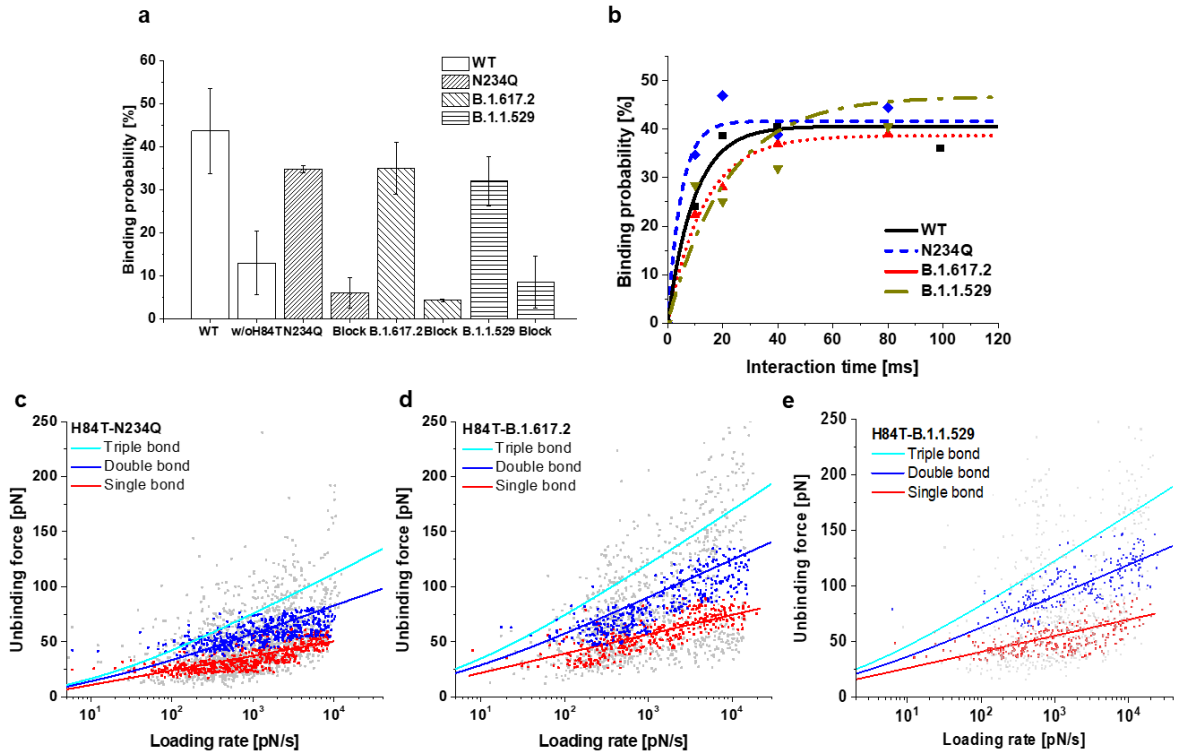

Figure S8. Single molecule force spectroscopy measurements. H84T-BanLec was immobilized onto surfaces and trimeric spike proteins were coupled to AFM tips. **a,** Binding activity and control experiments demonstrating the specificity of the interaction. Binding probability, presented as the percentage of force experiments displaying unbinding events, between H84T-BanLec and the spike of wild-type (WT), N234Q, B.1.617.2, and B.1.1.529 SARS-CoV-2 strains, respectively. Adjacent to the right of each binding activity experiment, control experiments using a surface only functionalized with PEG linker (without H84T, WT spike) or blocking experiments using pre-incubated spike coupled tip in H84T-BanLec solution for 20 min and adding H84T-BanLec (Block) into the measurement solution with N234Q, B.1.617.2 or B.1.1.529); a significant drop in the binding probability was seen in each case. **b,** Determination of kinetic on-rate between H84T-BanLec and the spike of WT, N234Q, B.1.617.2, and B.1.1.529 SARS-CoV-2 strains, respectively. Binding probability was plotted as a function of the interaction time. The solid line was the result of a least-square fit of a mono-exponential decay, assuming pseudo first-order kinetics. Plot of unbinding force versus loading rate for **c,** N234Q spike mutant **d,** B.1.617.2 spike trimer and **e,** B.1.1.529 spike trimer dissociating from H84T-BanLec. A Markov binding model computed the behavior of the double bond (blue) and triple bond (cyan) interactions, using parameters derived from the Bell and Evan's single-barrier model fit of the single bond (red). Related to Figures 4 and 5.

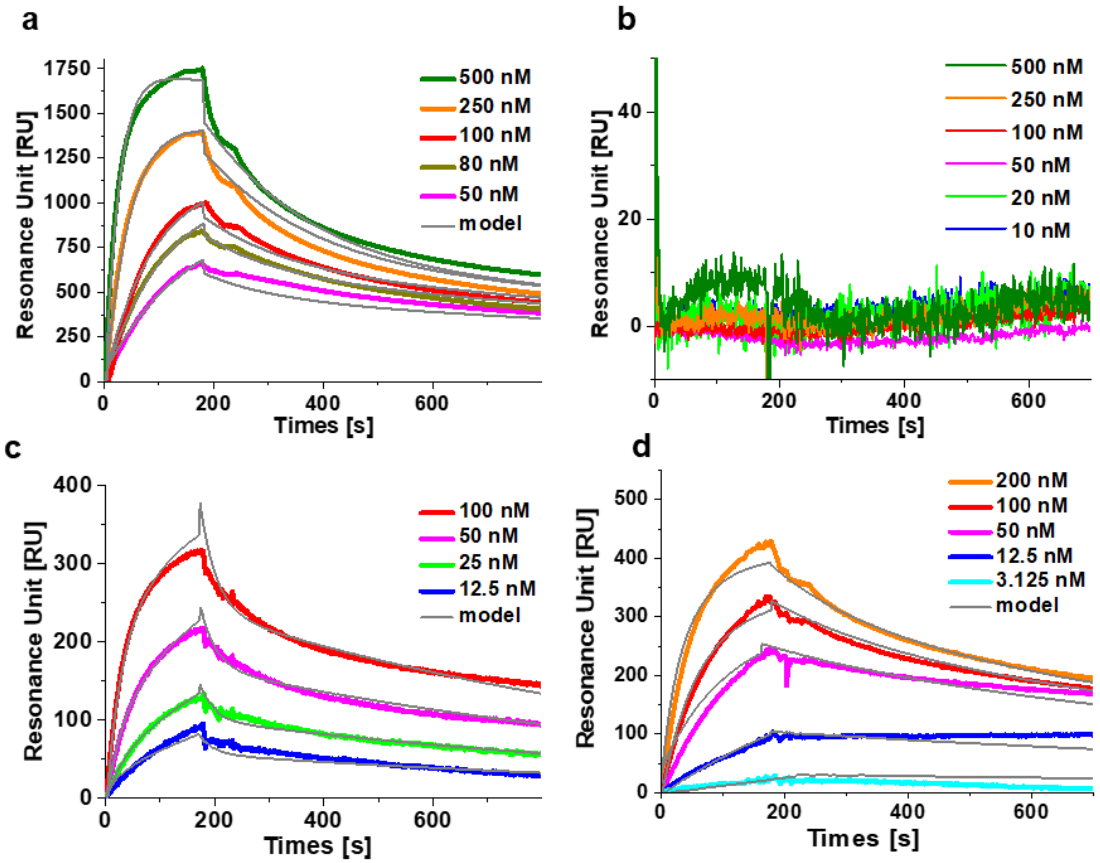

Figure S9. Surface plasmon resonance (SPR) measurements. H84T-BanLec was injected at the indicated concentrations to surfaces containing immobilized **a,** full-length trimeric N234Q spike mutant or **b,** receptor-binding domain to allow for binding (ascending parts), followed by wash out using buffer (descending parts) **c,** trimeric B.1.627.2 variant spike, and **d,** trimeric B.1.1.529 variant spike. Data were fitted using the bivalent binding model, consistent with H84T-BanLec being predominantly a dimer. To compare the binding of H84T-BanLec to the N234Q and B.1.627.2 spike proteins to that of the standard spike, see **Fig. 4H**. Related to Figures 4 and 5.

	Dynamic Force Spectroscopy (DFS)				Surface Plasmon Resonance (SPR)			
	H84T-BanLec /Spike trimer	H84T-BanLec /N234Q spike mutant	H84T-BanLec /B.1.617.2 trimer	H84T-BanLec /B.1.1.529 trimer	H84T-BanLec /Spike trimer	H84T-BanLec /N234Q spike mutant	H84T-BanLec /B.1.617.2 trimer	H84T-BanLec /B.1.1.529 trimer
$k_{off,\ 1}$ [1/s]	0.0457 ± 0.024	0.2585 ± 0.0135	0.0476 ± 0.0246	0.0314 ± 0.008	0.0262 ± 0.007	0.006 ± 0.0027	0.0249 ± 0.0031	0.0079 ± 0.0068
$k_{on,\ 1}$ [1/Ms]	$9.98 \times 10^4 \pm 5.18 \times 10^4$	$2.87 \times 10^5 \pm 0.66 \times 10^5$	$1.91 \times 10^5 \pm 0.52 \times 10^5$	$3.46 \times 10^4 \pm 0.23 \times 10^4$	$2.09 \times 10^4 \pm 0.25 \times 10^4$	$2.99 \times 10^4 \pm 0.31 \times 10^4$	$4.31 \times 10^4 \pm 0.23 \times 10^4$	$3.80 \times 10^4 \pm 1.41 \times 10^4$
K_D [M]	$4.6 \times 10^{-7} \pm 4.37 \times 10^{-7}$	$9.61 \times 10^{-7} \pm 2.68 \times 10^{-7}$	$2.54 \times 10^{-7} \pm 1.06 \times 10^{-7}$	$9.17 \times 10^{-7} \pm 3.16 \times 10^{-7}$	$1.28 \times 10^{-6} \pm 0.19 \times 10^{-6}$	$2.17 \times 10^{-7} \pm 1.14 \times 10^{-7}$	$5.76 \times 10^{-7} \pm 0.41 \times 10^{-7}$	$3.63 \times 10^{-7} \pm 4.23 \times 10^{-7}$
X_β [Å]	7.83 ± 0.60	7.30 ± 0.15	6.53 ± 2.28	6.28 ± 0.32				

Table S1. Quantification of parameters obtained with dynamic force spectroscopy (DFS) and surface plasmon resonance (SPR) methods. k_{on}, k_{off}, and K_D, are kinetic on-rate, kinetic off-rate, and equilibrium dissociation constant, respectively, of a single bond (DFS) or the first binding step (SPR). X_β denotes the distance of the activation barrier from the energy minimum along the pulling axis in DFS experiments. Related to Figures 4 and 5.